Dose-Rate Estimation using -Al2O3:C Chips: Aftermath

Kreutzer, Sebastian; Tribolo, Chantal; Martin, Loïc; Mercier, Norbert

Published in:
Ancient TL

Publication date:
2020

Citation for published version (APA):
Kreutzer, S., Tribolo, C., Martin, L., & Mercier, N. (2020). Dose-Rate Estimation using -Al_2O_3:C Chips: Aftermath. *Ancient TL*, *38*(1), 1-10. http://ancienttl.org/ATL_38-1_2020/ATL_38-1_Kreutzer_p1-10.pdf

Ancient TL

Dose-Rate Estimation using α-Al_2O_3:C Chips: Aftermath

Sebastian Kreutzer[1,2], Chantal Tribolo[1], Loïc Martin[3,1], Norbert Mercier[1]

[1]Geography & Earth Sciences, Aberystwyth University, Aberystwyth, Wales, United Kingdom
[2]IRAMAT-CRP2A, UMR 5060, CNRS-Université Bordeaux Montaigne, Pessac, France
[3]Scottish Universities Environmental Research Centre, East Kilbride, United Kingdom

Corresponding Author:sebastian.kreutzer@aber.ac.uk

Received: April 23, 2020; in final form: May 25, 2020

Abstract

We present additional experiments for α-Al_2O_3:C chips used to estimate *in situ* γ-dose rates. Our contribution supplements the article by Kreutzer et al. (2018) and presents results from previously announced follow-up experiments. (1) We investigate the divergent γ-dose rate results we obtained from cross-check experiments for one reference site. (2) We discuss the origin of encountered large inter-aliquot scatter using results from low-level background and calibration measurements. (3) We show that the chip geometries vary considerably, which may partly contribute to additional inter-aliquot scatter, regardless of an overall good reproducibility of results. (4) We report new source-calibration results after replacing the β-source housing of our measurement system, which resulted in an increase of the source dose rate at the sample position by ca 37 %. *GEANT4* simulations show that the increased dose rate is likely caused by an unfortunate fabrication tolerance of the shutter in front of the β-source, which, in combination with the chip geometry, significantly contributes to the observed inter-aliquot scatter. (5) Finally, we introduce a newly developed shiny application we use at the IRAMAT-CRP2A to analyse α-Al_2O_3:C measurements. The application is open-source and freely available.

Keywords: Dosimetry, Al_2O_3:C, Luminescence

1. Introduction

Two years ago, Kreutzer et al. (2018) published an article outlining techniques and workflow to determine the environmental γ-dose rate with passive α-Al_2O_3:C chips (Akselrod et al., 1990a,b, 1993). The contribution included performance tests of the used *lexsyg SMART* (Richter et al., 2015) reader, newly developed software functions for the **R** (R Core Team, 2019) package 'Luminescence' (Kreutzer et al., 2012), an application example at the archaeological site Sierra de Atapuerca (e.g., Aguirre & Carbonell, 2001), and a cross-check of the so estimated γ-dose rates against four different references sites around Clermont-Ferrand (France) (Miallier et al., 2009). While the performance of the presented system proved satisfactory, we identified two issues as potential subjects to further tests:

1. The cross-check against the reference site 'PEP' (a granite block, cf. Miallier et al., 2009) yielded a γ-dose rate ca 13 % lower than expected. Kreutzer et al. (2018) argued that field evidence revealed a tube movement partly out of the granite block after storage, which may have caused the recorded lower γ-dose rate ($\dot{D}_\gamma$).

2. The observed relative standard deviation (three chips in each of the 21 dosimeter tubes) ranged from 1.1 % to 15.1 % for the application site Sierra de Atapuerca. The resulting average value of 5.1 % was much higher than the 0.2 % scatter observed in reproducibility tests in the laboratory.

In the best tradition of Ancient TL, our contribution compiles a lab report with results addressing these two previously encountered issues. Additionally, we present observations made in the course of our β-source calibrations after exchanging the source-module housing. The remainder briefly

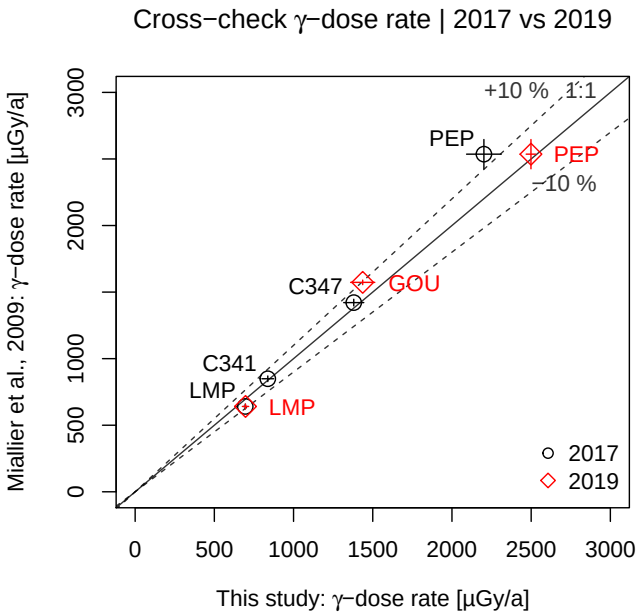

Figure 1. Natural γ-dose rates measured according to Kreutzer et al. (2018) against values tabulated in Miallier et al. (2009) in 2017 (black circles) (Kreutzer et al., 2018, their Fig. 8) and newly measured in 2019 (red diamonds). The solid black line indicates the 1:1 line, dashed lines the 10 % divergence from unity. For the measured chips we quoted the mean ± standard deviation of the mean. For the reference site values, uncertainties were taken from Miallier et al. (2009). Please note that in Kreutzer et al. (2018) we mixed up the labels for the sites LMP and C341. Here the labels are plotted correctly.

introduces an open-source shiny (Chang et al., 2019) application developed to analyse α-Al_2O_3:C measurements at the IRAMAT-CRP2A.

We will keep details on instrumentation, measurement protocol and analysis procedure to a minimum. For full details, we refer to Kreutzer et al. (2018), which is available as an open-access article. For all presented measurements, we employed the same *lexsyg SMART* (Richter et al., 2015) luminescence reader we already used for the article by Kreutzer et al. (2018). For the data analysis we employed the **R** scripts from Kreutzer et al. (2018) in conjunction with the most recent version of the **R** package 'Luminescence' (Kreutzer et al., 2019). Data analysis and visualisation benefited from the **R** packages 'ggplot' (Wickham, 2009), 'gridExtra' (Auguie, 2017), 'readxl' (Wickham & Bryan, 2019), and 'khroma' (Frerebeau, 2019).

2. $\dot{D}_\gamma$ cross-check

Our first experiment concerned the divergent γ-dose rate ($\dot{D}_\gamma$) results we obtained from our cross-check experiments for the granite block 'PEP'. The $\dot{D}_\gamma$ measured with the α-Al_2O_3:C chips was ca 13 % lower than expected in comparison to the values quoted in Miallier et al. (2009). In summer 2018, new tubes with three chips each were stored at three reference sites: (1) 'PEP' (granite), (2) 'LMP' (basalt), and (3) the before not considered site 'GOU' (trachyandesite). The three sites cover a wide range of annual $\dot{D}_\gamma$ values allowing to re-evaluate the performance of the procedure by Kreutzer et al. (2018) from, LMP: (641 ± 18) μGy a^{-1}, over GOU: (1573 ± 17) μGy a^{-1}, up to PEP: (2536 ± 110) μGy a^{-1} (Miallier et al., 2009). The dosimeters were measured in February 2019, five days after their retrieval from the sites. In total, the environmental $\dot{D}_\gamma$s were recorded over 313 days (LMP, GOU), and 315 days (PEP).

The combined results of our measurements from 2017 and 2019 are displayed in Fig. 1. Our measurements from 2019 (red diamonds) exhibit $\dot{D}_\gamma$-values within 10 % of the expected $\dot{D}_\gamma$. These findings seem to confirm the hypothesis that the unexpected dose-rate offset measured for PEP was not random but likely related to a displacement of the sample tube after initial storage in the rock. However, below, we will discuss another possibility that will let appear this result coincidentally. We will show that the geometry of the chips in combination with the irradiation geometry, may have led to the discrepancy observed in 2017.

Besides, the data exhibit that the expected natural $\dot{D}_\gamma$-values can be sufficiently recovered. Sample LMP gave nearly identical results, with an overall recovery of 0.98 ± 0.09 (2017) vs. 1.00 ± 0.09 (2019) (quoted are arithmetic mean ± standard deviation). In summary (data 2017 and 2019, excluding the outlier for PEP from 2017), a natural $\dot{D}_\gamma$ can be recovered within ca 7 % from unity.

3. Cosmic-dose rate impact?

The second experiment targeted the inter-aliquot dispersion when chips are stored in a natural environment over a long period (> 1 day). Kreutzer et al. (2018) speculated that cosmic-rays might explain the dispersion of the dose values due to the storage orientation of the chips in the site. Horizontal stacking of the chips in the tube usually exposes a smaller surface towards the cardinal point than vertically stacked chips. Although cosmic-rays do not hit targets on the ground only in a 90° angle, the chip orientation may indeed play a role in the observed scatter. To test whether the chip orientation has a measurable impact on the $\dot{D}_\gamma$ scatter, we designed the following experiment.

Twenty-six chips, reset at 910 °C for 10 min in an external furnace, were placed in a home-made cuboid made out of radio-nuclide free polymethyl methacrylate (PMMA, acrylic glass) (Fig. 2). The cuboid has a footage of 100 × 80 mm and a total height of 60 mm and consists of two parts, a cover and a body. The cover is detachable, either to stack chips in a vertical or horizontal orientation in slots in the cuboid body. The slots size facilitate chips with a diameter up to 5.2 mm. The box design and the location of the slots within the cuboid ensured that the chips were not affected by external α and β-particles. Their contribution to the dose accumulated by the chips is negligible. All slots used were filled up to their maximum capacity with chips. The number of chips per slot varied due to different chip thickness (see Sec. 4). Scotch tape ensured that the chips did not move. The box cover and box body were glued and sealed with Scotch tape

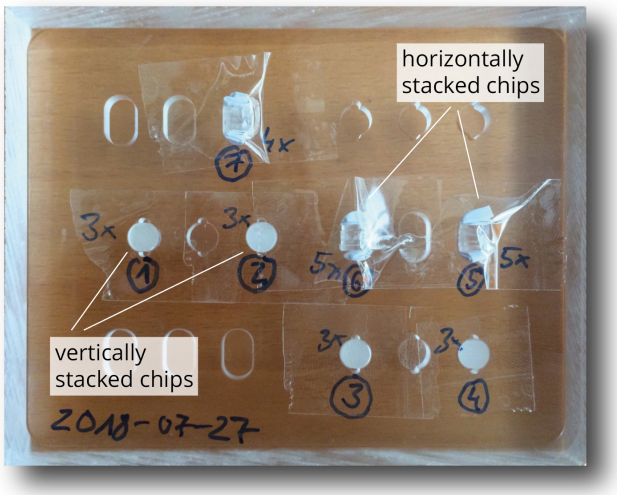

Figure 2. Top view photo of the bottom of the dosimeter storage cuboid made of radionuclide free acrylic glass. The cuboid has 18 positions, nine for horizontally and nine for vertically chip stacking. For our experiments, we used only seven positions (26 chips in total). The number of chips per position varied with chip thickness (four chips in position 7 vs five chips each in positions 5 and 6). Scotch tape on the top prevented the chips from moving. During the experiment, bottom and cover of the cuboid were glued together. The brownish background in the photo reflects the office table where the cuboid was placed on for the photo.

and enveloped in opaque bags to prevent light exposure. The cuboid was then placed in the low-background radiation lead castle in the cellar of the IRAMAT-CRP2A. This lead castle is the same that we use to store, temporarily, dosimeter tubes from the field, if they cannot be measured upon arrival.

The chips were stored for 361 days and then measured and analysed following the procedure outlined in Kreutzer et al. (2018). Figure 3 shows the results of this experiment for dose values derived from the green stimulated luminescence (GSL) signal and the subsequent thermal luminescence (TL) signal used to deplete the remaining luminescence. Black circles display results of the accumulated dose for chips orientated vertically, and red triangles illustrate horizontally stacked chips. It appears that the individual standard error[1] for vertically stacked chips are slightly higher than for chips stored horizontally. However, the main question is: *Does the distribution indicate two distinct dose groups correlated with the orientation of the chips in the cuboid?*

A two-sided Welch t-test returned a p-value of 0.04 (t = 2.17, df = 24). This result suggests a random difference between the two groups for a significance level of 1 %. However, a Q-Q plot (not shown) revealed that the distributions followed only vaguely normal distributions, which makes the application of a t-test debatable. An additionally performed two-sided Kolmogorov-Smirnov test returned a p-value of 0.14 (D = 0.43), also implying that the observed difference between the two orientation groups is random.

[1]The term "standard error" was used following the nomenclature used by Galbraith (1990).

As a side effect, with the described experiment, we were able to estimate the background-dose rate in our lead castle. The average accumulated dose over 26 chips amounted to $(155 \pm 23)\,\mu$Gy, which corresponds to an annual background-dose rate ($\dot{D}_\gamma + \dot{D}_{cosmic}$) of ca 157 μGy a^{-1}. In light of the minimum determination limit of ca 10 μGy estimated by Kreutzer et al. (2018) for the dosimetry system (OSL/TL reader and measurement protocol) used at the IRAMAT-CRP2A, it implies that dosimeter tube storage times of less than one month will not add a dose distinguishable from background noise.

Nevertheless, Fig. 3 indicates an additional grouping of aliquots, which does not appear to be related to the slot group positioning and the orientation of the chips in the cuboid. Moreover, the plot reveals a large scatter between chips in general (c_v of the full dataset: 14.5 %).

Over the years, we purchased batches of α-Al_2O_3:C chips from the same manufacturer varying slightly in diameter, thickness and colour (transparent, milky). For all measurements shown here and by Kreutzer et al. (2018), chips were not preselected but picked-up randomly from a box containing hundreds of chips of mixed batches. The reproducibility experiments by Kreutzer et al. (2018) did not reveal any particular problem with the chips or showed a particular correlation with an unknown variable.

While we cannot exclude that different batches have slightly different dose-response characteristics, additional measurements were made in order to double check the effect of varying chip geometry on the measured dose.

4. Chip geometry impact

We analysed 33 Al_2O_3:C chips placed in 11 tubes such as those described by Kreutzer et al. (2018) and inserted them for one year in the stratigraphic section of Border Cave, a Palaeolithic site in South Africa (e.g., Grün & Beaumont, 2001; Backwell et al., 2018). Each tube contained three chips; one additional tube was used as travel dosimeter. After the measurements, the thickness and diameter of each chip were measured (accuracy $\pm$ 0.01 mm). Figure 4 displays the variability of the chip geometry. We identified two major groups: (1) chips displaying thickness values between 0.78 mm and 0.80 mm and diameters between 5.01 mm and 5.16 mm, and (2) chips with higher thickness between 0.87 mm to 1.02 mm but narrower diameter (4.61 mm to 4.99 mm). A third group with a thickness similar to group (1) but with diameters in the same range as group (2) might be identifiable. Overall, diameter and thickness can vary from chip-to-chip by up to 12 % and 20 %, respectively.

The tubes were located in different places at Border Cave, and we did not expect similar D_γ-values for different tubes. However, the three chips within each tube should display statistically undistinguishable doses. In Fig. 5 we show the measured standardised dose as dependent variable of the chip volume (as aggregated variable of thickness and diameter); colours code different tubes. Figure 5A renders a picture similar to Fig. 4, the chips show two separate groups.

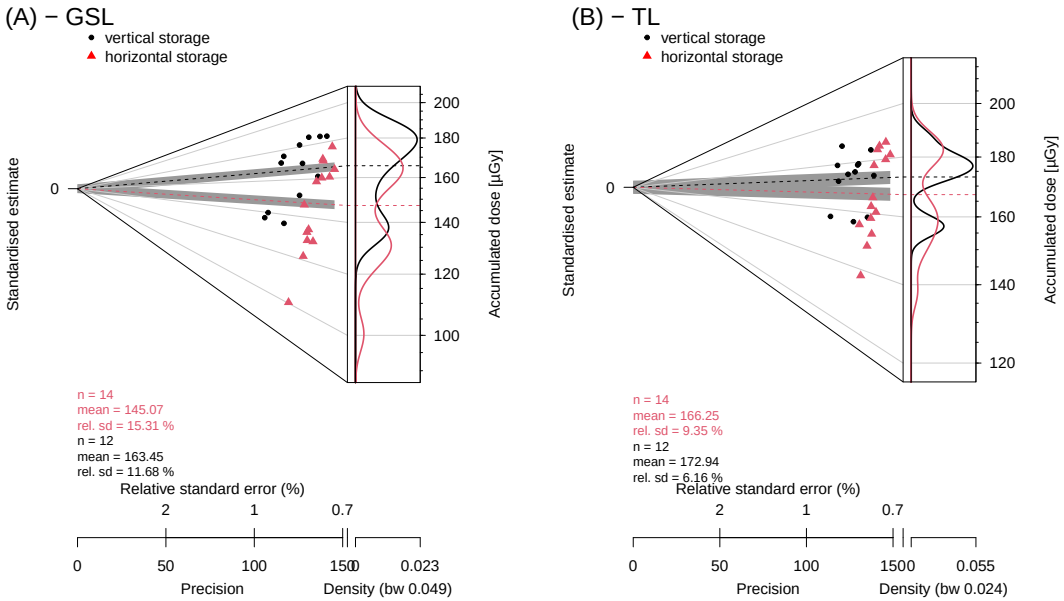

Figure 3. Abanico plots (Dietze et al., 2016) showing accumulated background doses after 361 days. Black circles indicate vertically, red triangles horizontally stacked chips. (A) D_e derived using the GSL signal, (B) D_e determined from the subsequent TL curve. In the latter case the obtained dose is not overall correct, but the scatter between the two groups can still be compared. For the interpretation of the term "relative standard error" as used in the plot we refer to Galbraith (1990).

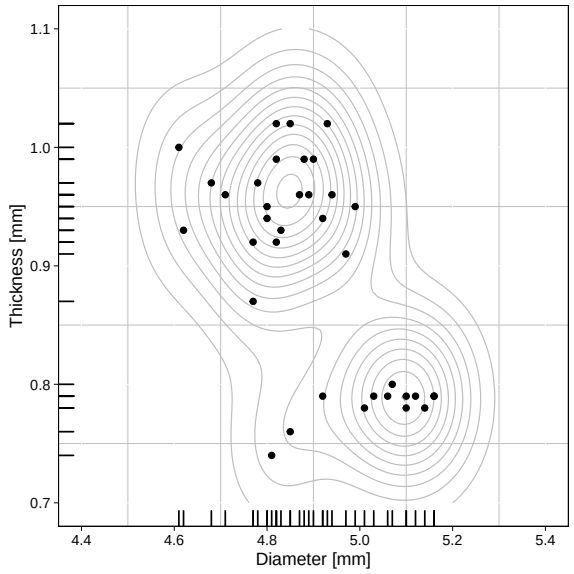

Figure 4. Diameter and thickness variation of the chips (n=33). Measurement uncertainties are too small to be displayed.

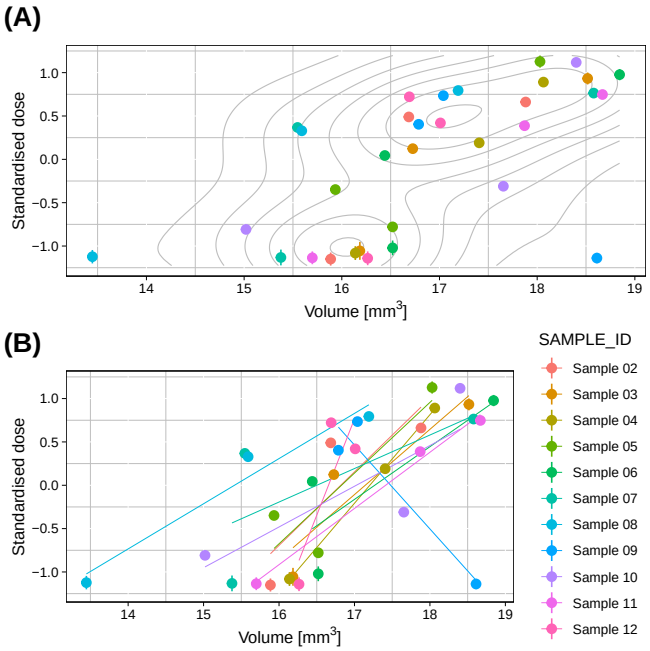

Figure 5. Standardised dose vs chip volume. (A) and (B) show the same values, with a different graphical representation. The solid lines in (B) are linear regression lines for each tube. Standardised dose values were calculated as follows: $d_{std} = (d_i - \bar{d})/\sigma$, with $\bar{d}$ being the average dose rate and σ the standard deviation.

Whether this difference in volume relates to real differences in doses can be seen in Fig. 5B. Here we have drawn regression lines separately for each tube. We observed, (1) a significant variability for the measured dose in each tube (10 % to 20 %), and (2) that this variation appears to correlate positively with the chip volume. Higher volumes seem to lead to higher doses. One tube (Sample 09, Fig. 5B), shows a negative correlation of volume with dose, which might be, however, related to the luminescence characteristics of this particular chip.

We checked similar plots for the diameter and the thickness instead of the aggregated variable volume (not shown). Using a regression analysis to understand the impact of thickness and diameter on the standardised dose, we found that, combined, both parameters explain 59.5 % (adjusted R^2) of the variance in the dataset. However, only the thickness has a significant impact on the explained variance. In other

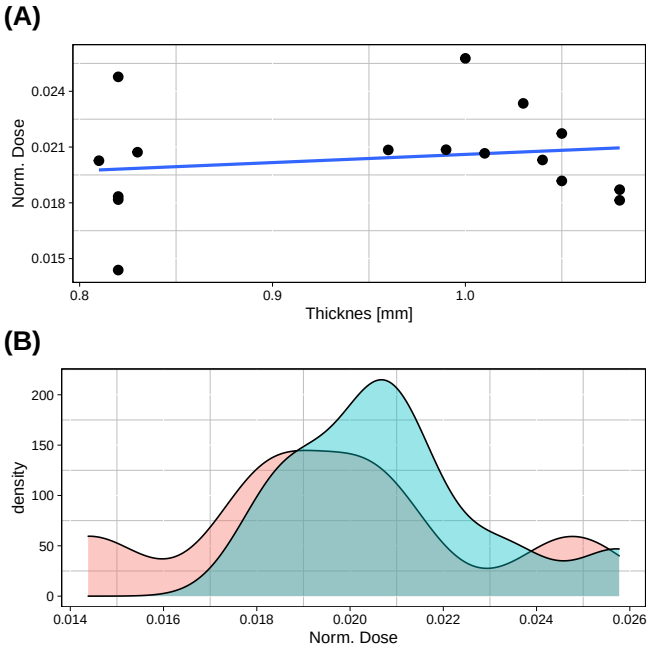

Figure 6. Apparent dose normalised to the storage duration vs chip thickness. (A) Displays a weak positive correlation between thickness and normalised dose. (B) shows the normalised dose groups (threshold: chip thickness 0.9 mm) as kernel density plots, both distributions overlap and are statistically indistinguishable (see *t*-test results).

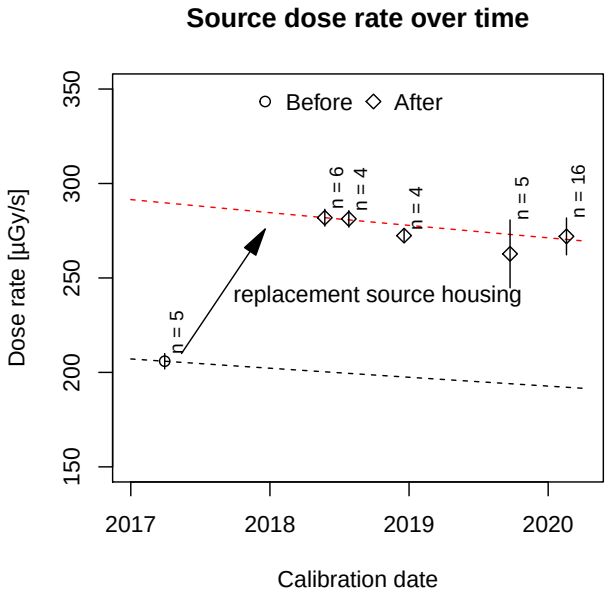

Figure 7. Source-calibration results over time. The dashed lines indicate the predicted dose-rate evolution of the ^{90}Sr/^{90}Y-source based in the first calibration point. The circle indicates the dose rate before, the diamonds the dose rates after the source housing was replaced. Dose-rate values refer to calibration measurements under the source with its shutter closed. Shown are mean ± standard deviation of the mean.

words, while differences in diameter may still have a small impact on the dose variance, the major driver appears to be the chip thickness. Hence, 40.5 % of the variance remain unexplained. The true dose (D_γ + D_{cosmic}) recorded in each tube should be independent of the chip thickness, given the travel range of natural γ-photons and cosmic-rays. The variability observed in the apparent dose for each set of the three chips may thus be linked to the irradiation in the luminescence reader. This consists of bremsstrahlung and high-energy electrons (Kreutzer et al., 2018), which are attenuated at the scale of a few millimetres (see Sec. 5). If this is the case, the source dose rate obtained through calibration measurements should be a function of the chip thickness.

Hence, we set up a new calibration experiment taking into account the chip thickness. The experimental design was similar to what was done by Kreutzer et al. (2018). We stored six tubes (three chips each), in the middle of a brick block with a well known γ-dose rate (Richter et al., 2010) available in the basement of the IRAMAT-CRP2A for periods of 140 days to 634 days.

Figure 6 displays the results of this experiment as thickness vs dose normalised to the storage duration. We removed two (out of 18 values) from the plot. One chip exhibited a dose ca two times higher than the highest dose value from the distribution and one chip could not be retrieved from the tube.

The chip thicknesses range similar to those values observed previously, i.e. between 0.81 mm and 0.83 mm for one group and between 0.96 mm and 1.08 mm for the second one.

While Fig. 6A indicates a weak positive correlation between chip thickness and normalised dose (r = 0.17), the two dose distributions (Fig. 6B) are statistically indistinguishable for a significance level of 5 % (two-sided Welch *t*-test, *p*-value: 0.367, *t* = -0.96, df = 7.7).

It must be noted here that, contrary to what was recommended in Kreutzer et al. (2018), the cups used for the measurements were not heated to 450 °C before the measurements. This may have induced some additional scatter. However, the mean dose rate is consistent with dose rates expected from previous experiments, where heating of the discs before the measurement was performed (see below).

5. Source-calibration and an unexpected dose-rate evolution

In summer 2018, a shutter failure of the β-source module in the *lexsyg SMART* required a source-housing exchange service. This requires that the ^{90}Sr/^{90}Y source (cf. Fig. 2 in Richter et al., 2012) is detached from the housing module (enveloped in a lead shield), which facilitates shutter and sensor electronics, before getting re-attached to the new housing. In theory, since the modules are certified and identical in design, such intervention should not alter the source dose rate.

To our surprise, a source calibration carried out immediately after the source-housing replacement showed a remarkable leap of the source-dose rate by 36.9 % (Fig. 7). At the same time, our routine source-calibrations using optically stimulated luminescence (OSL, Huntley et al., 1985) in

conjunction with the single-aliquot regenerated (SAR) dose protocol (Murray & Wintle, 2000) on quartz separates, also carried out after the replacement of the source housing, remained unsuspicious. We, therefore, repeated the calibration shortly after and again in 2019 applying the procedure outlined in Kreutzer et al. (2018) (including the irradiation time correction and cross-talk measurements) with fresh chips stored in the cubic brick block in the cellar of our laboratory (cf. Kreutzer et al., 2018; Richter et al., 2010). The last calibration (see results Sec. 4) was run in February 2020. Figure 4 displays all five source-calibration values rendering consistent within uncertainty after the exchange of the source housing. Moreover, Fig. 1 proves that our calibrations are overall correct since the results in 2019 and 2020 are consistent with the values from 2017 (after the replacement). Finally, the last calibration, for which the chip thickness was checked, suggests that the change in the dose rate is not related to the chip thickness (Sec. 4).

5.1. Additional *GEANT4* simulations

To determine the cause of the dose-rate change and estimate how dose is deposited as a function of the chip thickness, we ran additional *GEANT4* (Agostinelli et al., 2003) simulations on a dedicated multi-core server at the IRAMAT-CRP2A. We simulated an irradiation geometry similar to the one in the *lexsyg SMART* based on technical information provided to every customer by Freiberg Instruments. According to the manufacturer, both source housings (new and replaced one) were identical. However, the stainless steel shutter, which was produced by an external manufacturer, has a fabrication tolerance of ± 0.1 mm (pers. comm. Andreas Richter, Freiberg Instruments GmbH). In other words, the shutter can have a thickness between 0.9 mm and 1.1 mm. Based on this information and combined with our observations regarding the thickness of the chips presented above, we developed six scenarios to model the dose rate for shutter geometries of 0.9 mm, 1 mm, and 1.1 mm repeated for chips with a thickness of 0.8 mm and 1 mm.

The simulated irradiation spectrum (Fig. 8A) show that while the X-ray spectrum is not significantly affected by the thickness of the source shutter, the amount of incident β-particles range over approximately an order of magnitude. Lowest values are observed for a shutter of 1.1 mm thickness. Please note that Fig. 8A represents the six simulation scenarios, i.e. combinations of shutter thickness and chip thickness. However, the incident spectra cannot be affected by the chip thickness, and variations in the curves are random. Figure 8B shows the local dose-rate profile for the three shutter configurations. The curve shapes differ for the shutter geometries but are mostly similar for the different chip thicknesses. The corresponding chip dose rate is the respective average of these curves (Fig. 8C). For a shutter with a thickness of 0.9 mm the simulated dose rate between chips with a thickness of 1 mm and 0.8 mm deviates by 15.3 % and only 5.8 % for a shutter with a thickness of 1.1 mm.

We ran additional tests for the varying chip diameters (we list $\dot{D}_{Sr-90}$ for extreme chip geometries in the appendix). We found only a weak impact of the shutter thickness on the induces dose rates. This finding confirms our results from Sec. 4 where we showed that differences in chip thickness explain more dose variance than differences in chip diameters. While a thicker shutter shows a dose rate less dependable on the chip geometry, it also reduces the dose rate by a factor of ca 2 per 1 mm. Vice versa, the results leave little doubt that our new source housing module has a thinner shutter installed, hence we observed the jump of the dose rate after the replacement service.

The simulated dose rates are at least 50 % lower than the measured values in Fig. 7. To some extent, this discrepancy is likely a result of the simplified geometry used for the simulation (e.g., instead of a cup, we used a disc-like geometry for the sample carrier). Nonetheless, we consider our simulations as qualitatively correct regarding the impact of the shutter thickness on the dose rate induced in chips of different thickness.

In conjunction with the observations presented in Sec. 4 these findings render a comprehensive picture, and demand a critical reflection on our procedure to measure Al_2O_3:C chips.

1. The simulated irradiation spectra questions our, so far applied, approach to consider geometry effects in the irradiation field negligible.
2. Depending on the shutter thickness, the passing high-energy β-particles induce considerable chip geometry related dose rates.
3. Although the source calibration results itself seem to show only a weak correlation with chip thickness (Fig. 7), the presented results strongly indicate that the dose scatter observed between chips is mainly an effect caused by the irradiation geometry in the measurement system.

Despite the overall acceptable reproducibility of natural $\dot{D}_\gamma$s (Sec. 2), in light of our findings we suggest the following additional measures when using Al_2O_3:C chips for *in situ* dose-rate measurements:

1. Different batches of chips must not be mixed and kept well separated.
2. Users should double-check their chip geometries and recalibrate their systems for their respective geometries.
3. It appears to be advisable, to double the number of tubes stored per sampling position (e.g., two tubes instead of one), so that the mean dose-rate can be obtained with higher confidence.
4. Since it appears that a thicker shutter can markedly reduce the geometry effects, it might be desirable to liaise with the manufacturer when ordering a new system or exchange the source housing. This might be also advisable from the radiation protection point of view.

Overall, the findings show that the origin of the scatter is not easy to fathom, and our results still may not tell the entire story. Compared to data measured in 2017, perhaps the chips

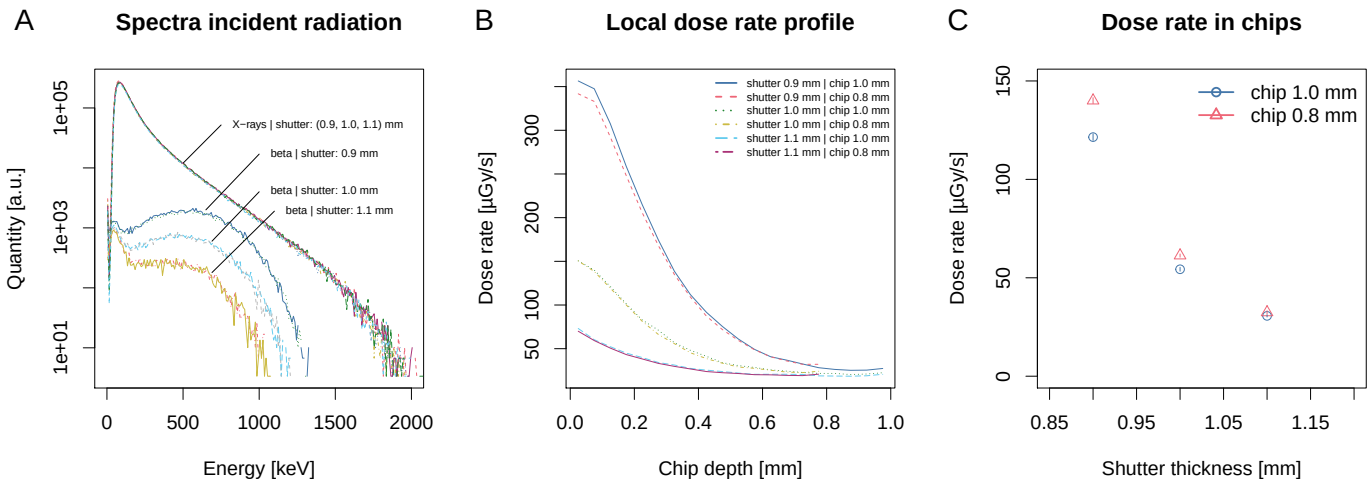

Figure 8. Results of the *GEANT4* simulations. The figures show the effect of different irradiation scenarios in the *lexsyg SMART* reader used for the measurements. (A) displays the spectra of the incident particles (here β-particles and X-ray photons) at the sample position for different shutter thicknesses. Colours code shutter geometries and chip geometries (1.0 mm and 0.8 mm). (B) Local dose rate profile for different irradiation geometries. (C) Induced chip dose rate as a dependent of the shutter thickness for two different chip geometries.

also suffer from some kind of degeneration contributing to the observed higher dose dispersion. Such a degeneration might be caused by the regular heating of the chips to 910 °C before being shipped to the field. However, such treatment is applied to empty the deep electron traps (Akselrod et al., 1990a), and even though this is considered a routine procedure, not being reported hazardous to the chips (Erfurt et al., 2000; Kalchgruber & Wagner, 2006; Yukihara & McKeever, 2011), one may wonder whether it causes an unexpected ageing of the chips. We are going to investigate this issue in the future.

In summary, the presented results emphasize another time that users should always remain suspicious regarding their measurement equipment (see also Kreutzer et al., 2017), in particular when dealing with new or modified systems. Moreover, the results underline another time the importance of regular source calibrations (for a recent discussion see Tribolo et al., 2019).

6. The Al_2O_3:C Analysis App

Along with their article, Kreutzer et al. (2018) deployed three new **R** functions for the package 'Luminescence' tailored to analyse calibration and routine dosimeter measurements. However, setting knowledge on **R** and the **R** package 'Luminescence' in particular as a prerequisite for analysing dosimeter measurements put up a barrier to a quick adoption in a laboratory that regularly hosts international guest researchers, students, and interns. Consequently, we decided to develop a so-called, shiny (Chang et al., 2019) application called 'Al_2O_3:C Analysis App' which is a graphical user interface to the **R** function `analyse_Al2O3C_Measurement()` in the 'Luminescence' package. In our laboratory, the application runs on a local *RStudio*® (`https://www.rstudio.com`) server. Users access the application platform-independent using a state-of-the-art browser of their choice. The 'Al_2O_3:C Analysis App' has three main panels for data import, data analysis, and post-processing including an export option of the results (cf. Fig. 9).

The user has various possibilities to interact with the software, such as copy & paste tabulated values or swipe through the graphical output. Furthermore, the software automatically provides access to all available system calibration datasets (cf. Kreutzer et al., 2018), such as irradiation time correction, cross-talk correction, and source calibration, so far they are stored on the same server. The software sets no limits regarding the number of datasets to access, and multiple reader data are accessible within the same environment. If no calibration datasets are available, data can still be analysed, but are of limited scientific value. Own calibration datasets, produced using the procedure detailed in Kreutzer et al. (2018) can be uploaded and used at any time during one session.

The application is available free of charge via `https://github.com/crp2a/Al2O3_AnalysisApp`. As usual, we published the software under the General Public Licence (GPL-3), which means it can be even modified and adapted following the licence conditions.

7. Conclusions

We presented new findings from follow-up experiments testing the reliability of our workflow employed to measure the environmental γ-dose rate using passive dosimeters detailed by Kreutzer et al. (2018). If tested against natural reference sites, a known γ-dose rate is reproducible within ca 7 %. Our cosmic-ray experiment, however, indicated a much larger scatter between aliquots, which can amount up to 15 % in low-level background environments. We did not find a statistical significant correlation between the chip orientation and the recorded dose. *GEANT4* simulations gave

Figure 9. Screenshots of the shiny application 'Al_2O_3:C Analysis App' freely available at https://github.com/crp2a/Al2O3_AnalysisApp.

evidence that the majority of the scatter can be explained by different chip geometries in conjunction with an unfortunate fabrication tolerance of the shutter in front of the radioactive source. The replacement of the source housing led to an increased dose-rate induced in the chips. The thinner shutter, (1) increased the number of high-energy β -particles passing the shutter, and (2) caused a higher dependency of the induced dose rate on the chip thickness. This explained why we observed (1) an increased dose-rate induced in the chips by ca 37 % after the replacement of the source housing and (2) a difference in the induced dose rate of at least 15 % for chips of 0.8 mm and 1 mm while irradiated in the reader. We suggested a couple of measures to reduce the inter-aliquot scatter, and with this systematic effects likely not related to the real dose-rate variations in the field. However, this aspect will receive further attention in the future.

Nevertheless, the employed experiments, along with the good reproducibility of calibration results, show the still overall justified applicability of our approach. The presented shiny application may serve those who do not want to learn **R** first before analysing their data.

Finally, our contribution falls in line with uncounted articles, many of them in Ancient TL, addressing potential sources of systematic uncertainties when determining luminescence ages. These days, more and more sophisticated numerical methods, such as Bayesian modelling (e.g., Combès et al., 2015; Combès & Philippe, 2017; Philippe et al., 2019), are adopted by the luminescence community. For those methods, a profound understanding and quantification of sources of systematic uncertainties are not just a 'nice to have', but an essential prerequisite to deploy their full potential and deliver correct overall calculations.

Author contributions

SK prepared the initial manuscript and developed the shiny application, CT organised the re-check at the reference sites and ran part of the measurements, calibrations as well as the first data analysis. LM designed, ran and analysed the *GEANT4* simulations. NM initiated and supervised the work. All authors discussed the results and equally contributed to the final manuscript.

Acknowledgements

We thank Dr Yukihara for valuable comments on our manuscript. Didier Miallier is thanked another time for his valuable support with the dosimeters at the reference sites around Clermont-Ferrand. This work received financial support by the LaScArBx LabEx, a programme supported by the ANR - n° ANR-10-LABX-52, and by the project DAPRES_LA_FEM, funded by the Region Nouvelle Aquitaine. While the manuscript was completed, SK has received funding from the European Union's Horizon 2020 research and innovation programme under the Marie Skłodowska-Curie grant agreement No 844457.

Appendix

Table 1. Values for $\dot{D}_{Sr-90}$ for extreme chip configurations.

	Shutter thickness [mm]		
Parameter	**0.9**	**1.0**	**1.1**
$\dot{D}_{C_{max}}$ [μGy s^{-1}]	154.9	65.3	34.0
(uncert. - 95 % CL)	(3.0)	(0.4)	(0.3)
$\dot{D}_{C_{min}}$ [μGy s^{-1}]	106.7	49.6	29.6
(uncert. - 95 % CL)	(1.1)	(0.5)	(0.5)
Diff. (C_{max}, C_{min})	**31 %**	**24 %**	**13 %**
(uncert. - 95 % CL)	(2 %)	(1 %)	(2 %)

C_{min}: tck. = 1.14 mm | ρ = 5.03 g cm^{-3} | dim. = 5.11 mm
C_{min}: tck. = 0.80 mm | ρ = 4.17 g cm^{-3} | dim. = 4.73 mm
CL: confidence level | tck.: thickness | dim.: diameter

References

Agostinelli, S., Allison, J., Amako, K., Apostolakis, J., Araujo, H., Arce, P., Asai, M., Axen, D., Banerjee, S., Barrand, G., Behner, F., Bellagamba, L., Boudreau, J., Broglia, L., Brunengo, A., Burkhardt, H., Chauvie, S., Chuma, J., Chytracek, R., Cooperman, G., Cosmo, G., Degtyarenko, P., Dell'Acqua, A., Depaola, G., Dietrich, D., Enami, R., Feliciello, A., Ferguson, C., Fesefeldt, H., Folger, G., Foppiano, F., Forti, A., Garelli, S., Giani, S., Giannitrapani, R., Gibin, D., Gómez Cadenas, J. J., González, I., Gracia Abril, G., Greeniaus, G., Greiner, W., Grichine, V., Grossheim, A., Guatelli, S., Gumplinger, P., Hamatsu, R., Hashimoto, K., Hasui, H., Heikkinen, A., Howard, A., Ivanchenko, V., Johnson, A., Jones, F. W., Kallenbach, J., Kanaya, N., Kawabata, M., Kawabata, Y., Kawaguti, M., Kelner, S., Kent, P., Kimura, A., Kodama, T., Kokoulin, R., Kossov, M., Kurashige, H., Lamanna, E., Lampén, T., Lara, V., Lefebure, V., Lei, F., Liendl, M., Lockman, W., Longo, F., Magni, S., Maire, M., Medernach, E., Minamimoto, K., Mora de Freitas, P., Morita, Y., Murakami, K., Nagamatu, M., Nartallo, R., Nieminen, P., Nishimura, T., Ohtsubo, K., Okamura, M., O'Neale, S., Oohata, Y., Paech, K., Perl, J., Pfeiffer, A., Pia, M. G., Ranjard, F., Rybin, A., Sadilov, S., Di Salvo, E., Santin, G., Sasaki, T., Savvas, N., Sawada, Y., Scherer, S., Sei, S., Sirotenko, V., Smith, D., Starkov, N., Stoecker, H., Sulkimo, J., Takahata, M., Tanaka, S., Tcherniaev, E., Safai Tehrani, E., Tropeano, M., Truscott, P., Uno, H., Urban, L., Urban, P., Verderi, M., Walkden, A., Wander, W., Weber, H., Wellisch, J. P., Wenaus, T., Williams, D. C., Wright, D., Yamada, T., Yoshida, H., and Zschiesche, D. *Geant4—a simulation toolkit*. Nuclear Instruments and Methods in Physics Research Section A: Accelerators, Spectrometers, Detectors and Associated Equipment, 506(3): 250–303, 2003. doi: 10.1016/S0168-9002(03)01368-8.

Aguirre, E. and Carbonell, E. *Early human expansions into Eurasia: The Atapuerca evidence*. Quaternary International, 75(1): 11–18, 2001. doi: 10.1016/S1040-6182(00)00073-2.

Akselrod, M. S., Kortov, V. S., Kravetsky, D. J., and Gotlib, V. I. *Highly Sensitive Thermoluminescent Anion-Defective Alpha-Al_2O_3:C Single Crystal Detectors*. Radiation Protection Dosimetry, 32(1): 15–20, 1990a. doi: 10.1093/oxfordjournals.rpd.a080715.

Akselrod, M. S., Kortov, V. S., Kravetsky, D. J., and Gotlib, V. I. *Highly Sensitive Thermoluminescent Anion-Defect Alpha-Al_2O_3:C Single Crystal Detectors*. Radiation Protection Dosimetry, 33(1-4): 119–122, 1990b. doi: 10.1093/oxfordjournals.rpd.a080771.

Akselrod, M. S., Kortov, V., and Gorelova, E. *Preparation and Properties of $\alpha - Al_2O_3 : C$*. Radiation Protection Dosimetry, 47(1-4): 159–164, 1993. doi: 10.1093/oxfordjournals.rpd.a081723.

Auguie, B. *gridExtra: Miscellaneous Functions for "Grid" Graphics*, 2017. URL https://CRAN.R-project.org/package=gridExtra. R package version 2.3.

Backwell, L. R., d'Errico, F., Banks, W. E., de la Peña, P., Sievers, C., Stratford, D., Lennox, S. J., Wojcieszak, M., Bordy, E. M., Bradfield, J., and Wadley, L. *New Excavations at Border Cave, KwaZulu-Natal, South Africa*. Journal of Field Archaeology, 0 (0): 1–20, 2018. doi: 10.1080/00934690.2018.1504544.

Chang, W., Cheng, J., Allaire, J., Xie, Y., and McPherson, J. *shiny: Web Application Framework for R*, 2019. URL https://CRAN.R-project.org/package=shiny. R package version 1.3.2.

Combès, B. and Philippe, A. *Bayesian analysis of individual and systematic multiplicative errors for estimating ages with stratigraphic constraints in optically stimulated luminescence dating*. Quaternary Geochronology, 39: 24–34, 2017. doi: 10.1016/j.quageo.2017.02.003.

Combès, B., Philippe, A., Lanos, P., Mercier, N., Tribolo, C., Guérin, G., Guibert, P., and Lahaye, C. *A Bayesian central equivalent dose model for optically stimulated luminescence dating*. 28: 62–70, 2015. doi: 10.1016/j.quageo.2015.04.001.

Dietze, M., Kreutzer, S., Burow, C., Fuchs, M. C., Fischer, M., and Schmidt, C. *The abanico plot: visualising chronometric data with individual standard errors*. Quaternary Geochronology, 31: 12–18, 2016. doi: 10.1016/j.quageo.2015.09.003.

Erfurt, G., Krbetschek, M. R., Trautmann, T., and Stolz, W. *Radioluminescence (RL) behaviour of Al_2O_3:C-potential for dosimetric applications*. Radiation Measurements, 32(5–6): 735–739, 2000. doi: 10.1016/S1350-4487(00)00052-4.

Frerebeau, N. *khroma: Colour Schemes for Scientific Data Visualization*. Université Bordeaux Montaigne, Pessac, France, 2019. URL https://CRAN.R-project.org/package=khroma. R package version 1.3.0.

Galbraith, R. F. *The radial plot: Graphical assessment of spread in ages*. International Journal of Radiation Applications and Instrumentation. Part D. Nuclear Tracks and Radiation Measurements, 17(3): 207–214, 1990. doi: 10.1016/1359-0189(90)90036-W.

Grün, R. and Beaumont, P. *Border Cave revisited: a revised ESR chronology*. Journal of Human Evolution, 40(6): 467–482, 2001. doi: 10.1006/jhev.2001.0471.

Huntley, D. J., Godfrey-Smith, D. I., and Thewalt, M. L. W. *Optical dating of sediments*. Nature, 313: 105–107, 1985. doi: 10.1038/313105a0.

Kalchgruber, R. and Wagner, G. A. *Separate assessment of natural beta and gamma dose-rates with TL from single-crystal chips*. Radiation Measurements, 41(2): 154–162, 2006. doi: 10.1016/j.radmeas.2005.04.002.

Kreutzer, S., Schmidt, C., Fuchs, M. C., Dietze, M., Fischer, M., and Fuchs, M. *Introducing an R package for luminescence dating analysis*. Ancient TL, 30(1): 1–8, 2012. URL http://ancienttl.org/ATL_30-1_2012/ATL_30-1_Kreutzer_p1-8.pdf.

Kreutzer, S., Murari, M. K., Frouin, M., Fuchs, M., and Mercier, N. *Always remain suspicious: a case study on tracking down a technical artefact while measuring IR-RF*. Ancient TL, 35(1): 20–30, 2017. URL http://www.ecu.edu/cs-cas/physics/ancient-timeline/upload/ATL_35-1_Kreutzer_p20-30.pdf.

Kreutzer, S., Martin, L., Guérin, G., Tribolo, C., Selva, P., and Mercier, N. *Environmental Dose Rate Determination Using a Passive Dosimeter: Techniques and Workflow for alpha-Al_2O_3:C Chips*. Geochronometria, 45: 56–67, 2018. doi: 10.1515/geochr-2015-0086.

Kreutzer, S., Burow, C., Dietze, M., Fuchs, M. C., Schmidt, C., Fischer, M., and Friedrich, J. *Luminescence: Comprehensive Luminescence Dating Data Analysis*, 2019. URL https://CRAN.R-project.org/package=Luminescence. R package version 0.9.3.

Miallier, D., Guérin, G., Mercier, N., Pilleyre, T., and Sanzelle, S. *The Clermont radiometric reference rocks: a convenient tool for dosimetric purposes*. Ancient TL, 27: 37–44, 2009. URL http://ancienttl.org/ATL_27-2_2009/ATL_27-2_Miallier_p37-44.pdf.

Murray, A. S. and Wintle, A. G. *Luminescence dating of quartz using an improved single-aliquot regenerative-dose protocol*. Radiation Measurements, 32(1): 57–73, 2000. doi: 10.1016/S1350-4487(99)00253-X.

Philippe, A., Guérin, G., and Kreutzer, S. *BayLum - An R package for Bayesian analysis of OSL ages: An introduction*. Quaternary Geochronology, 49: 16–24, 2019. doi: 10.1016/j.quageo.2018.05.009.

R Core Team. *R: A Language and Environment for Statistical Computing*. Vienna, Austria, 2019. URL https://r-project.org.

Richter, D., Dombrowski, H., Neumaier, S., Guibert, P., and Zink, A. C. *Environmental gamma dosimetry with OSL of -Al2O3:C for in situ sediment measurements*. Radiation Protection Dosimetry, 141(1): 27–35, 2010. doi: 10.1093/rpd/ncq146.

Richter, D., Pintaske, R., Dornich, K., and Krbetschek, M. R. *A novel beta source design for uniform irradiation in dosimetric applications*. Ancient TL, 30(2): 57–63, 2012. URL http://ancienttl.org/ATL_30-2_2012/ATL_30-2_Richter_p57-64.pdf.

Richter, D., Richter, A., and Dornich, K. *Lexsyg smart — a luminescence detection system for dosimetry, material research and dating application*. Geochronometria, 42(1): 202–209, 2015. doi: 10.1515/geochr-2015-0022.

Tribolo, C., Kreutzer, S., and Mercier, N. *How reliable are our beta-source calibrations?* Ancient TL, 37(1): 1–10, 2019. URL http://ancienttl.org/ATL_37-1_2019/ATL_37-1_Tribolo_p1-10.pdf.

Wickham, H. *ggplot2: Elegant Graphics for Data Analysis*. Springer New York, New York, NY, 2009.

Wickham, H. and Bryan, J. *readxl: Read Excel Files*, 2019. URL https://CRAN.R-project.org/package=readxl. R package version 1.3.1.

Yukihara, E. G. and McKeever, S. W. S. *Optically Stimulated Luminescence*. Optically Stimulated Luminescence. Wiley, 2011.

Reviewer

Eduardo Gardenali Yukihara

Reviewer comment

At this temperature [meant are 910°C] one does not expect much senstivitiy change, but with time it has been observed that a dead layer develops due to diffusion of oxygen. This can be tested by comparing the sensitvitiy of the chips with the sensitivity of polished chips exposed to α-particles.